Applied Physics Letters

Large topological Hall effect in an easy-cone ferromagnet $(Cr_{0.9}B_{0.1})Te$

Cite as: Appl. Phys. Lett. **117**, 052409 (2020); https://doi.org/10.1063/5.0018229
Submitted: 12 June 2020 • Accepted: 24 July 2020 • Published Online: 07 August 2020

Yangkun He, Johannes Kroder, Jacob Gayles, et al.

Applied Physics Letters ARTICLE scitation.org/journal/apl

Large topological Hall effect in an easy-cone ferromagnet $(Cr_{0.9}B_{0.1})Te$

Cite as: Appl. Phys. Lett. **117**, 052409 (2020); doi: 10.1063/5.0018229
Submitted: 12 June 2020 · Accepted: 24 July 2020 ·
Published Online: 7 August 2020

View Online Export Citation CrossMark

Yangkun He,[a] Johannes Kroder, Jacob Gayles, Chenguang Fu, Yu Pan, Walter Schnelle, Claudia Felser, and Gerhard H. Fecher

AFFILIATIONS

Max Planck Institute for Chemical Physics of Solids, D-01187 Dresden, Germany

[a]Author to whom correspondence should be addressed: yangkun.he@cpfs.mpg.de

ABSTRACT

The Berry phase understanding of electronic properties has attracted special interest in condensed matter physics, leading to phenomena such as the anomalous Hall effect and the topological Hall effect. A non-vanishing Berry phase, induced in momentum space by the band structure or in real space by a non-coplanar spin structure, is the origin of both effects. Here, we report a sign conversion of the anomalous Hall effect and a large topological Hall effect in $(Cr_{0.9}B_{0.1})Te$ single crystals. The spin reorientation from an easy-axis structure at high temperature to an easy-cone structure below 140 K leads to conversion of the Berry curvature, which influences both, anomalous and topological, Hall effects in the presence of an applied magnetic field and current. We compare and summarize the topological Hall effect in four categories with different mechanisms and have a discussion into the possible artificial fake effect of the topological Hall effect in polycrystalline samples, which provides a deep understanding of the relation between the spin structure and Hall properties.

In condensed matter physics, Berry phases have enabled a wider understanding of many physical concepts and phenomena, such as chiral anomalies,[1,2] magnetic monopoles,[3] and the anomalous Nernst effect.[4] Among them, the intrinsic anomalous Hall effect (AHE) requires the absence of time reversal symmetry and the orbital degeneracy to be lifted. The former not only is usually seen in ferromagnetic systems but also can be found in specific antiferromagnetic systems. The latter not only is due to relativistic effects such as the spin–orbit interaction but can also be induced by a non-collinear magnetic spin texture.[5,6] The combination of these phenomena leads to the momentum-space Berry curvature as a linear response to an applied electric field.[7,8] However, a real-space Berry phase originating from non-coplanar spin texture or magnetic topological excitations like skyrmions[9] with non-zero scalar spin chirality can also play the role of the magnetic field and contribute to the Hall signal, referred to as the topological Hall effect (THE).[10]

A topological Hall effect was first observed in skyrmions in non-centrosymmetric materials, such as the B20 compounds MnSi[11,12] and FeGe,[13,14] in which it is stabilized by the Dzyaloshinskii–Moriya interaction. In these cubic systems, the topological Hall resistivity is usually as small as 10^{-3}–10^{-2} $\mu\Omega$ cm. In centrosymmetric materials with uniaxial magnetic anisotropy, such as MnNiGa,[15] the biskyrmionic phase shows a large topological Hall effect of 0.15 $\mu\Omega$ cm. A topological Hall effect was also observed in systems with a non-coplanar antiferromagnetic spin structure, such as Mn_5Si_3,[16] MnP,[17] and YMn_6Sn_6.[18] Under an applied magnetic field strong enough for a metamagnetic or spin-flop transition, the (partially) antiferromagnetic coupled or canted spins align to the field direction due to the Zeeman energy, a process during which a large topological Hall resistivity of up to 10^{-1} $\mu\Omega$ cm has been observed. More recently, a topological Hall effect was also observed during the magnetization process along the hard axis of ferromagnets, such as in strong uniaxial Cr_5Te_8[19] and Fe_3GeTe_2[20] with a magnetic field applied in-plane. None of these materials, however, shows a topological Hall effect with a field along the easy axis (*c*-axis). This suggests a complex behavior during magnetization along the hard axis in ferromagnets. Many Mn-based Heusler compounds crystallize in an inverse structure[21–25] and have a non-collinear spin structure at low temperature. They exhibit a topological Hall effect that belongs to a mixed type of the above two cases. Recently, the THE was also reported in frustrated magnets.[26,27]

The topological Hall effect is one of the characteristics of skyrmions, and electrical transport is easy to measure. Therefore, it can be used to select materials for potential skyrmion applications. In

addition, the topological Hall effect can be used to confirm some non-coplanar spin structures without the need for expensive neutron studies.

Ferromagnetism exists in a large range of compositions in $Cr_{1-x}Te$ ($0 < x < 0.4$) with different Curie temperatures T_c and saturation magnetization M_s.[28] These compounds share a similar hexagonal structure, with Cr vacancies in every second Cr layer, while the Te layer is fully occupied. The vacancies induce small deviations from the hexagonal symmetry, leading to monoclinic Cr_3Te_4, trigonal Cr_2Te_3, and trigonal or monoclinic Cr_5Te_8. Trigonal Cr_5Te_8 is a strong uniaxial ferromagnet with a magneto-crystalline anisotropy constant K_1 of 0.8 MJ m^{-3}.[19,29] However, for materials with a higher Cr concentration and smaller anisotropy ($K_1 < 0.5$ MJ m^{-3}),[30,31] the magnetic structure is much more complicated. A canted ferromagnetic structure at low temperature was observed by neutron diffraction[32] and magnetization measurements,[28] which could lead to a possible real-space Berry phase and a topological Hall effect, providing a candidate material for skyrmion bubbles. In a previous study, we reported the magnetic structure of $(Cr_{0.9}B_{0.1})Te$.[33] Owing to the difficulty in synthesizing stoichiometric CrTe, the chromium vacancies are filled by boron, stabilizing the hexagonal structure as well as shifting the Fermi energy to modify the magnetism. The magnetic moment changes from collinear along c at high temperature to an easy-cone structure below the spin-reorientation transition temperature $T_{SR} = 140$ K. The tilt angle varies with temperature.

Here, we report the magneto-electronic transport properties of $(Cr_{0.9}B_{0.1})Te$ single crystals. The spin reorientation leads to a change in the Berry curvature, which significantly influences both, anomalous and topological, Hall effects depending on the applied magnetic field and current direction.

Single crystals of $(Cr_{0.9}B_{0.1})Te$ were grown by an annealing process followed by water quenching. The details of the crystal growth, composition, crystal structure, magnetic properties, and electronic structure are published in Ref. 33. The longitudinal and Hall resistivities were measured using a Quantum Design PPMS 9 by a standard four- or five-probe method.

$(Cr_{0.9}B_{0.1})Te$ crystallizes in a $B8_1$ structure (prototype: NiAs, hP4, $P6_3mmc$, 194) with alternating Cr and Te layers. The lattice constants are $a = 4.0184(6)$ Å and $c = 6.2684(7)$ Å. It is assumed that B replaces only Cr atoms of every second Cr layer. A collinear spin structure with an easy axis along c is observed at high temperature, whereas the magnetic moments localized at the Cr atoms become gradually tilted away from the c-axis at temperatures below 140 K.

The electric transport properties of $(Cr_{0.9}B_{0.1})Te$ single crystals are shown in Fig. 1 with $H//c$ [0001], $I//$ab plane [01-10] in Figs. 1(a)–1(c) and $H//ab$ plane [2-1-10], $I//c$ [0001] in Figs. 1(d)–1(f). Along both the c-axis and the ab plane, the longitudinal resistance shows a metallic behavior with a kink at $T_c = 336$ K, although the value in the ab plane is almost twice as large as that along the c-axis. The small residual-resistance ratio (RRR) is about 1.7 in-plane and 2.1 along the c-axis, indicating a large number of dislocations (vacancies or B atoms) inside the crystals. For magnetization along the c-axis, the magnetoresistance is almost zero, and as the field increases further, its value gradually decreases during heating to −1.5% at 300 K under 3 T due to spin-disorder scattering. However, the magnetoresistance is positive (1.5%) in the ab plane at 2 K during magnetization. With this additional effect, the negative magnetoresistance region at 3 T rises to above 200 K.

$(Cr_{0.9}B_{0.1})Te$ also exhibits a large, anisotropic anomalous Hall effect that depends strongly on temperature. When the applied field direction is along the c-axis, the anomalous Hall resistivity ρ_{AHE} is positive at high temperature with a collinear spin structure. However, it decreases during cooling and then changes its sign at T_{SR}, finally reaching −2.3 μΩ cm at 2 K, as shown in Fig. 1(c). When the field is in-plane, as shown in Fig. 1(f), the anomalous Hall effect is always negative and changes during cooling from −3.5 μΩ cm at 300 K to about −0.7 μΩ cm at 2 K. Skew scattering is the dominant mechanism of the anomalous Hall effect for both $I//ab$ and $I//c$,[19] as shown in the linear fitting of ρ_{AHE} vs longitudinal resistivity in the supplementary material. ρ_{AHE} offsets the trend when the temperature approaches T_c. The skew-scattering mechanism confirms $(Cr_{0.9}B_{0.1})Te$ as a bad metal with a large number of defects.

The total Hall effect can be regarded as the sum of the ordinary Hall effect due to the Lorenz force, the anomalous, and the topological Hall effect using the following formula for the Hall resistivity:

$$\rho_H = R_0 B + R_s \mu_0 M + \rho_{THE}, \quad (1)$$

where R_0 and R_s are the ordinary and anomalous Hall coefficients, respectively. The fitted ordinary Hall resistivity is negligible, indicating a high charge carrier density of more than 10^{22} cm^{-3}; therefore, it is not shown here. A low mobility of <1 cm^2 V^{-1} s^{-1} further demonstrates that it is a bad metal, which is also confirmed by the low residual resistivity ratio (RRR) and the low thermal conductivity of 3.8 W K^{-1} m^{-1} at 300 K. When the field is applied along the c-axis, R_s changes its sign during cooling, whereas it remains negative with the field along the a-axis, as shown in the supplementary material.

Moreover, the Hall signal during magnetization causes an additional effect, namely, the topological Hall effect, when $H//$[2-1-10] and $I//$[0001] with the easy-cone structure at low temperature, as shown in Fig. 2. At 250 K, with the collinear spin structure, there is no topological Hall effect. However, it appears below T_{SR} of 140 K. At 2 K, the value is as large as 0.21 μΩ cm. A similar result is observed when both the current and the field are in two in-plane perpendicular directions. A large topological Hall effect appears near saturation, when the easy-cone structure has already been destroyed by the applied magnetic field. Note that the in-plane magnetization curve below 140 K is not linear before saturation, with a kink at around 0.2 T (supplementary material), which is also the field at which the topological Hall effect starts to show a large value. This indicates a non-coplanar spin structure before saturation, with a solid angle Ω showing spin chirality as sketched in Fig. 3.

However, when the field is parallel to the c-axis, the topological Hall effect is too small to be distinguished from the noise. This can be explained by the lack of a non-coplanar intermediate phase during magnetization along the c-axis, as indicated by the absence of a kink in the magnetization curve (see the supplementary material). The domain wall motion and spin reorientation occur simultaneously during magnetization instead. This collinear spin structure does not give rise to an additional contribution to the Hall signal from the Berry curvature with $\Omega = 0$. Similar phenomena have been observed in Cr_5Te_8[19] and Fe_3GeTe_2,[20] which also show a topological Hall effect when the field is along the hard axis rather than the easy c-axis due to the non-coplanar spin structure.

Figure 4 shows the phase diagram according to the above data with the field in-plane. Here, T_c and T_{SR} are collected from the $M(T)$

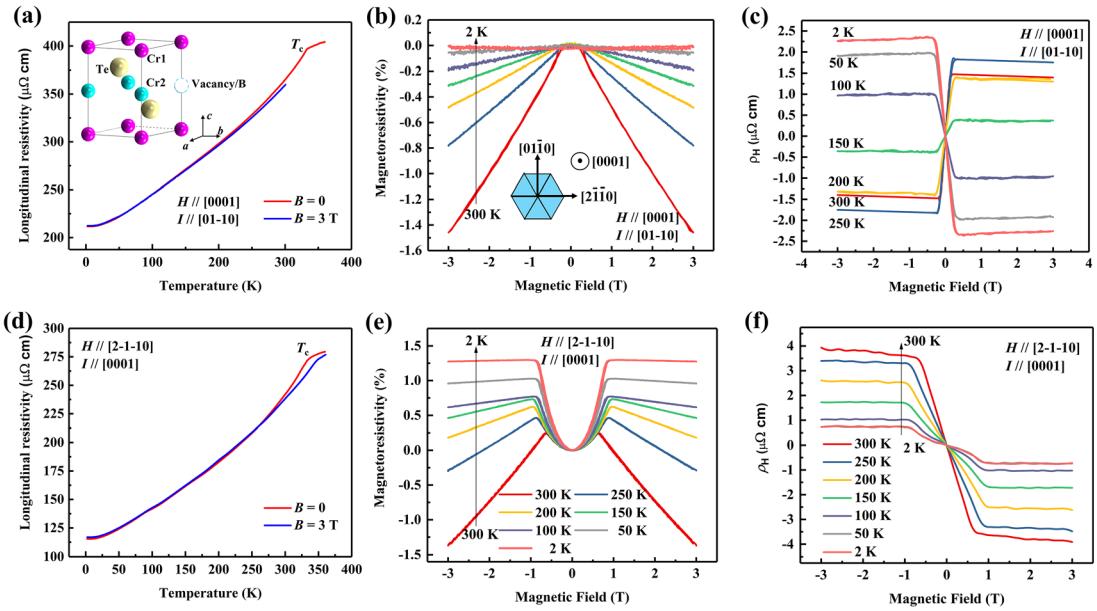

FIG. 1. Transport properties of $(Cr_{0.9}B_{0.1})Te$. (a) and (d) Longitudinal resistance. (b) and (e) Magnetoresistivity at 2–300 K. (c) and (f) Hall signal at 2–300 K. The demagnetizing factors here are approximately 0.40 and 0.65, respectively. The crystal structure is shown in the inset in (a).

curves, whereas the saturation field $\mu_0 H_s$ and the maximum field of the easy cone are collected from the $M(H)$ curves. It is clearly shown that the topological Hall effect appears at low temperature with a non-coplanar spin structure near saturation, when the spin is already shifted away from the initial cone.

We compare materials exhibiting a topological Hall effect in Table I. Generally, a large topological Hall effect requires a large magnetic field (see the supplementary material). The first category consists of the skyrmion materials. However, in general, the topological Hall effect induced by skyrmions is small. The cubic B20 compounds, such as MnSi[11,12] or FeGe,[13,14] only exhibit a topological Hall resistivity of 10^{-3}–10^{-2} $\mu\Omega$ cm. In $Mn_{1.4}PtSn$ above the spin-reorientation temperature, no topological Hall effect was found,[23] although skyrmions still existed.[34] The second category covers the

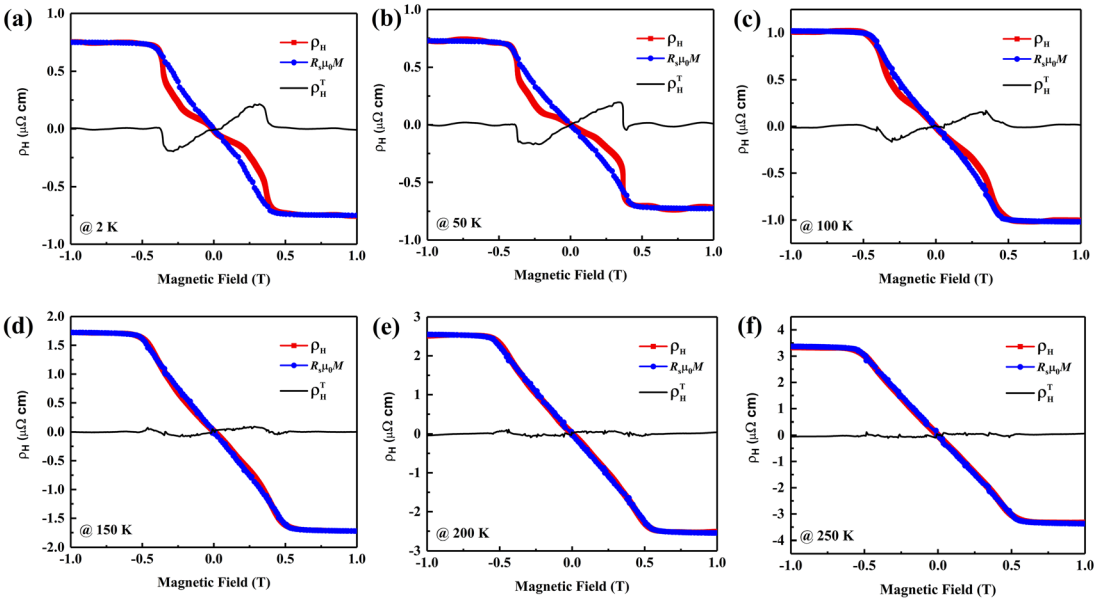

FIG. 2. Topological Hall effect of $(Cr_{0.9}B_{0.1})Te$ with *H*//[2-1-10] and *I*//[0001]. The demagnetizing effect has already been corrected here to remove the possibility of an artificial effect. (a)–(f) correspond to different temperatures from 2 K to 250 K, respectively.

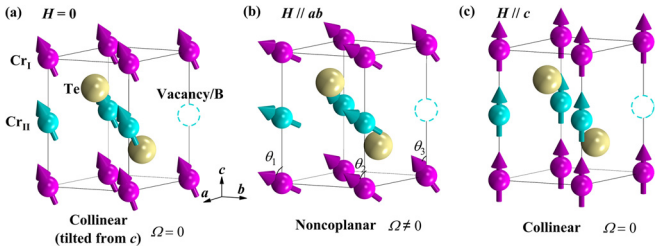

FIG. 3. Schematic magnetic and crystal structures of $(Cr_{0.9}B_{0.1})Te$ with (a) $H = 0$, (b) $H//ab$ plane, and (c) $H//c$. The moment is tilted from c and collinear in the ground state. The in-plane field leads to a non-coplanar spin structure with different tilted angles before saturation. The moment is collinear with the c-axis magnetic field.

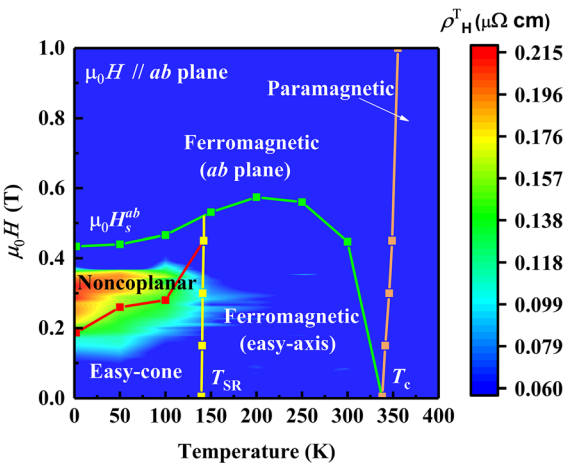

FIG. 4. Phase diagram of $(Cr_{0.9}B_{0.1})Te$ with the in-plane field.

possibility to realize metamagnetic or spin-flop transitions under applied magnetic fields in antiferromagnetic materials with a non-coplanar spin structure, as in the cases of Mn_5Si_3,[16] MnP,[17] and YMn_6Sn_6.[18] The third category covers magnetization from the hard axis, including Cr_5Te_8,[19] Fe_3GeTe_2,[20] and $(Cr_{0.9}B_{0.1})Te$. Many Mn-based Heusler compounds[21–25,35] have combined materials from all three categories. The topological Hall effects for the second and third categories are larger, with a large magnetic field, depending on the exchange coupling strength or magnetocrystalline anisotropy.

$(Cr_{0.9}B_{0.1})Te$ belongs to the third group and is one of the materials that can achieve a large anomalous Hall effect with a mild field owing to its small magnetocrystalline anisotropy. Note that the topological Hall resistivity of 0.21 $\mu\Omega$ cm is already comparable to the anomalous Hall resistivity of 0.75 $\mu\Omega$ cm. Larger values of the topological Hall effect are also observed in thin films,[36] which disappear when the thickness increases, indicating that the topological Hall effect is sensitive to the lattice constant, which is easily affected by strain. The small applied field is due to vanishing small single-ion anisotropy of Cr^{3+} ions ($3d^3$) with a negligible orbital moment.[33] Note that B significantly increases the Cr moment from 2.7 μ_B in the binary compound[28] to 3.1 μ_B here and decreases the magnetocrystalline anisotropy K_1 from 500 kJ m^{-3}[31] to −100 kJ m^{-3} at 2 K. This reduced field is important for potential applications.

The findings also allow us to interpret transport data from previously reported polycrystalline materials. We propose a *topological-like anomalous Hall effect* (topological AHE) that originates in polycrystals from two magnetic sublattices with different anisotropy constants, the values of which are approximately the same magnitude, but of opposite sign. We simulated a textured structure (80%c + 20%a) as an example using the data at 300 K in Fig. 1, as shown in the supplementary information. *Note that there is no topological Hall effect at this temperature.* The magnetization along the c-axis saturates fast, dominating the initial magnetization curve and the anomalous Hall effect (positive). However, after saturation in the "c"-texture in a higher field, an additional anomalous Hall effect only emerges from the "a"-texture, giving a negative contribution. As a result, a bump, namely, a topological-like anomalous Hall effect, appears near saturation. The topological-like anomalous Hall resistivity is 1.3 $\mu\Omega$ cm after fitting and, thus, much larger than the real topological Hall resistivity observed at low temperature. Dijkstra *et al.*[28] also reported Hall measurements on polycrystalline $Cr_{0.9}Te$ and $Cr_{0.8}Te$. Both samples, especially $Cr_{0.8}Te$, showed similar behavior of two kinks before saturation, which can now be explained by topological and topological-like anomalous Hall effects. The first kink might come from the competition between anomalous Hall effects with different signs, whereas the second kink should come from the topological Hall effect of the noncoplanar spin structure. Interestingly, this topological-like anomalous Hall effect has also been realized in films in which two materials with opposite signs of the anomalous Hall effect were selected.[37] Our study points out that this can be realized in one material as well. Owing to the topological-like anomalous Hall effect, great care should be taken with the transport properties of polycrystalline materials with an anisotropic crystal structure to exclude the possibility of an 'artificial topological Hall effect'. For this reason, some polycrystalline materials without texture, especially those with high magnetocrystalline anisotropy, are not included in Table I.

In conclusion, the spin reorientation transition at 140 K has a significant effect on the transport properties of $(Cr_{0.9}B_{0.1})Te$. The non-

TABLE I. Comparison of different categories of materials showing a topological Hall effect.

Materials	MnSi, FeGe	Mn_5Si_3, MnP, YMn_6Sn_6	Cr_5Te_8, Fe_3GeTe_2, $Cr_{0.9}B_{0.1}Te$	$Mn_{1.4}PtSn$, Mn_2RhSn
Ground state	Helical (AFM)	Non-collinear AFM	FM	Non-collinear FM
Process	Skyrmion	Metamagnetic transition	Hard-axis magnetization	Mixture
Field direction	All	All	Hard axis	All
Max THE ($\mu\Omega$ cm)	10^{-3}–10^{-2}	10^{-1}–10^{0}	10^{-2}–10^{1}	10^{-2}–10^{-1}
Magnetic field	Small	Large	Anisotropy dependent	Anisotropy dependent

coplanar spin structure at low temperature leads to a non-vanishing Berry phase, further causing a highly anisotropic anomalous Hall effect and a topological Hall effect that strongly depends on the field direction. Consequently, a sign change of the anomalous Hall effect and a large topological Hall resistivity of 0.21 $\mu\Omega$ cm are observed. Our study provides a deep understanding of the non-coplanar magnetic structure and topological Hall effect.

See the supplementary material for the mechanism of the anomalous Hall effect, topological-like anomalous Hall effect, magnetization curves, and comparison of the topological Hall effect with other materials.

This work was financially supported by the European Research Council Advanced Grant (No. 742068) "TOPMAT," the European Union's Horizon 2020 Research and Innovation Programme (No. 824123) "SKYTOP," the European Union's Horizon 2020 Research and Innovation Programme (No. 766566) "ASPIN," the Deutsche Forschungsgemeinschaft (Project-ID No. 258499086) "SFB 1143," the Deutsche Forschungsgemeinschaft (Project-ID No. FE 633/30-1) "SPP Skyrmions," and the DFG through the Würzburg–Dresden Cluster of Excellence on Complexity and Topology in Quantum Matter ct.qmat (EXC 2147, Project-ID No. 39085490).

DATA AVAILABILITY

Data are available on request from the authors.

REFERENCES

[1]E. Liu, Y. Sun, N. Kumar, L. Muechler, A. Sun, L. Jiao, S. Y. Yang, D. Liu, A. Liang, Q. Xu, J. Kroder, V. Süß, H. Borrmann, C. Shekhar, Z. Wang, C. Xi, W. Wang, W. Schnelle, S. Wirth, Y. Chen, S. T. B. Goennenwein, and C. Felser, "Giant anomalous Hall effect in a ferromagnetic kagome-lattice semimetal," Nat. Phys. **14**, 1125 (2018).
[2]J. Gooth, A. C. Niemann, T. Meng, A. G. Grushin, K. Landsteiner, B. Gotsmann, F. Menges, M. Schmidt, C. Shekhar, V. Süß, R. Hühne, B. Rellinghaus, C. Felser, B. Yan, and K. Nielsch, "Experimental signatures of the mixed axial–gravitational anomaly in the Weyl semimetal NbP," Nature **547**, 324 (2017).
[3]Z. Fang, N. Nagaosa, K. S. Takahashi, A. Asamitsu, R. Mathieu, T. Ogasawara, H. Yamada, M. Kawasaki, Y. Tokura, and K. Terakura, "The anomalous Hall effect and magnetic monopoles in momentum space," Science **302**, 92–95 (2003).
[4]A. Sakai, Y. P. Mizuta, A. A. Nugroho, R. Sihombing, T. Koretsune, M. T. Suzuki, N. Takemori, R. Ishii, D. Nishio-Hamane, R. Arita, P. Goswami, and S. Nakatsuji, "Giant anomalous Nernst effect and quantum-critical scaling in a ferromagnetic semimetal," Nat. Phys. **14**, 1119 (2018).
[5]S. Nakatsuji, N. Kiyohara, and T. Higo, "Large anomalous Hall effect in a non-collinear antiferromagnet at room temperature," Nature **527**, 212 (2015).
[6]X. Wang, Z. Feng, P. Qin, H. Yan, X. Zhou, H. Guo, Z. Leng, W. Chen, Q. Jia, Z. Hu, H. Wu, X. Zhang, C. Jiang, and Z. Liu, "Integration of the noncollinear antiferromagnetic metal Mn_3Sn onto ferroelectric oxides for electric-field control," Acta Mater. **181**, 537 (2019).
[7]N. Nagaosa, J. Sinova, S. Onoda, A. H. MacDonald, and N. P. Ong, "Anomalous Hall effect," Rev. Mod. Phys. **82**, 1539 (2010).
[8]K. Manna, Y. Sun, L. Muechler, J. Kübler, and C. Felser, "Heusler, Weyl and Berry," Nat. Rev. Mater. **3**, 244 (2018).
[9]A. Fert, N. Reyren, and V. Cros, "Magnetic skyrmions: Advances in physics and potential applications," Nat. Rev. Mater. **2**, 17031 (2017).
[10]N. Nagaosa and Y. Tokura, "Topological properties and dynamics of magnetic skyrmions," Nat. Nanotechnol. **8**, 899–911 (2013).
[11]A. Neubauer, C. Pfleiderer, B. Binz, A. Rosch, R. Ritz, P. G. Niklowitz, and P. Böni, "Topological Hall effect in the a phase of MnSi," Phys. Rev. Lett. **102**, 186602 (2009).
[12]Y. Li, N. Kanazawa, X. Z. Yu, A. Tsukazaki, M. Kawasaki, M. Ichikawa, X. F. Jin, F. Kagawa, and Y. Tokura, Phys. Rev. Lett. **110**, 117202 (2013).
[13]N. A. Porter, J. C. Gartside, and C. H. Marrows, "Scattering mechanisms in textured FeGe thin films: Magnetoresistance and the anomalous Hall effect," Phys. Rev. B **90**, 024403 (2014).
[14]N. Kanazawa, M. Kubota, A. Tsukazaki, Y. Kozuka, K. S. Takahashi, M. Kawasaki, M. Ichikawa, F. Kagawa, and Y. Tokura, "Discretized topological Hall effect emerging from skyrmions in constricted geometry," Phys. Rev. B **91**, 041122(R) (2015).
[15]W. Wang, Y. Zhang, G. Xu, L. Peng, B. Ding, Y. Wang, Z. Hou, X. Zhang, X. Li, E. Liu, S. Wang, J. Cai, F. Wang, J. Li, F. Hu, G. Wu, B. Shen, and X. X. Zhang, "A centrosymmetric hexagonal magnet with superstable biskyrmion magnetic nanodomains in a wide temperature range of 100–340 K," Adv. Mater. **28**, 6887–6893 (2016).
[16]C. Sürgers, G. Fischer, P. Winkel, and H. V. Löhneysen, "Large topological Hall effect in the non-collinear phase of an antiferromagnet," Nat. Commun **5**, 3400 (2014).
[17]Y. Shiomi, S. Iguchi, and Y. Tokura, "Emergence of topological Hall effect from fanlike spin structure as modified by Dzyaloshinsky–Moriya interaction in MnP," Phys. Rev. B **86**, 180404(R) (2012).
[18]Q. Wang, Q. Yin, S. Fujitsu, H. Hosono, and H. Lei, "Near-room-temperature giant topological Hall effect in antiferromagnetic Kagome metal YMn_6Sn_6," arXiv:1906.07986v1.
[19]Y. Wang, J. Yan, J. Li, S. Wang, M. Song, J. Song, Z. Li, K. Chen, Y. Qin, L. Ling, H. Du, L. Cao, X. Luo, Y. Xiong, and Y. Sun, "Magnetic anisotropy and topological Hall effect in the trigonal chromium tellurides Cr_5Te_8," Phys. Rev. B **100**, 024434 (2019).
[20]Y. Wang, C. Xian, J. Wang, B. Liu, L. Ling, L. Zhang, L. Cao, Z. Qu, and Y. Xiong, "Anisotropic anomalous Hall effect in triangular itinerant ferromagnet Fe_3GeTe_2," Phys. Rev. B **96**, 134428 (2017).
[21]K. G. Rana, O. Meshcheriakova, J. Kübler, B. Ernst, J. Karel, R. Hillebrand, E. Pippel1, P. Werner, A. K. Nayak, C. Felser, and S. S. P. Parkin, "Observation of topological Hall effect in Mn_2RhSn films," New J. Phys. **18**, 085007 (2016).
[22]Y. Li, B. Ding, X. Wang, H. Zhang, W. Wang, and Z. Liu, "Large topological Hall effect observed in tetragonal Mn_2PtSn Heusler thin film," Appl. Phys. Lett. **113**, 062406.
[23]P. Vir, J. Gayles, A. S. Sukhanov, N. Kumar, F. Damay, Y. Sun, J. Kübler, C. Shekhar, and C. Felser, "Anisotropic topological Hall effect with real and momentum space Berry curvature in the antiskyrmion-hosting Heusler compound $Mn_{1.4}PtSn$," Phys. Rev. B **99**, 140406(R) (2018).
[24]P. Swekis, A. Markou, D. Kriegner, J. Gayles, R. Schlitz, W. Schnelle, S. T. B. Goennenwein, and C. Felser, "Topological Hall effect in thin films of $Mn_{1.5}PtSn$," Phys. Rev. Mater. **3**, 013001(R) (2019).
[25]V. Kumar, N. Kumar, M. Reehuis, J. Gayles, A. S. Sukhanov, A. Hoser, F. Damay, C. Shekhar, P. Adler, and C. Felser, "Detection of antiskyrmions by topological Hall effect in Heusler compounds," Phys. Rev. B **101**, 014424 (2020).
[26]T. Kurumaji, T. Nakajima, M. Hirschberger, A. Kikkawa, Y. Yamasaki, H. Sagayama, H. Nakao, Y. Taguchi, T. Arima, and Y. Tokura, "Skyrmion lattice with a giant topological Hall effect in a frustrated triangular-lattice magnet," Science **365**, 914–918 (2019).
[27]H. Li, B. Ding, J. Chen, Z. Li, Z. Hou, E. Liu, H. Zhang, X. Xi, G. Wu, and W. Wang, "Large topological Hall effect in a geometrically frustrated kagome magnet Fe_3Sn_2," Appl. Phys. Lett **114**, 192408 (2019).
[28]J. Dijkstra, H. H. Weitering, C. F. Van Bruggen, C. Haas, and R. A. de Groot, "Band-structure calculations, and magnetic and transport properties of ferromagnetic chromium tellurides (CrTe, Cr_3Te_4, Cr_2Te_3," J. Phys.: Condens. Matter **1**, 9141 (1989).
[29]X. H. Luo, W. J. Ren, and Z. D. Zhang, "Magnetic properties and magnetocaloric effect of a trigonal Te-rich Cr_5Te_8 single crystal," J. Magn. Magn. Mater. **445**, 37–43 (2018).

[30]G. B. Street, E. Sawatzky, and K. Lee, "Magnetic properties of vapor grown crystals of hexagonal chromium telluride," J. Phys. Chem. Solids **34**, 1453–1455 (1973).
[31]T. Hirone and S. Chiba, "On the magnetic anisotropy of single crystal of chromium telluride," J. Phys. Soc. Jpn. **15**, 1991 (1960).
[32]A. F. Andersen, "The magnetic structure of Cr_2Te_3, Cr_3Te_4, and Cr_5Te_6," Acta Chem. Scand. **24**, 3495–3509 (1970).
[33]Y. He, G. H. Fecher, J. Kroder, H. Borrmann, X. Wang, L. Zhang, C. Kuo, C. Liu, C. Chen, K. Chen, F. Choueikani, P. Ohresser, A. Tanaka, Z. Hu, and C. Felser, "Easy-cone magnetic structure in $(Cr_{0.9}B_{0.1})Te$," Appl. Phys. Lett. **116**, 102404 (2020).
[34]A. K. Nayak, V. Kumar, T. Ma, P. Werner, E. Pippel, R. Sahoo, F. Damay, U. K. Rößler, C. Felser, and S. S. P. Parkin, "Magnetic antiskyrmions above room temperature in tetragonal Heusler materials," Nature. **548**, 561 (2017).
[35]B. M. Ludbrook, G. Dubuis, A. H. Puichaud, B. J. Ruck, and S. Granville, "Nucleation and annihilation of skyrmions in Mn_2CoAl observed through the topological Hall effect," Sci. Rep. **7**, 13620 (2017).
[36]D. Zhao, L. Zhang, I. A. Malik, M. Liao, W. Cui, X. Cai1, C. Zheng, L. Li, X. Hu, D. Zhang, J. Zhang, X. Chen, W. Jiang, and Q. Xue, "Observation of unconventional anomalous Hall effect in epitaxial CrTe thin films," Nano Res. **11**, 3116 (2018).
[37]A. Gerber, "Interpretation of experimental evidence of the topological Hall effect," Phys. Rev. B **98**, 214440 (2018).